Measurement and Characterization of Helicopter Noise at Different Altitudes

Michael E. Watts
NASA Langley Research Center
Hampton, VA

Eric Greenwood
NASA Langley Research Center
Hampton, VA

James H. Stephenson
US Army Aviation Development Directorate
Hampton, VA

ABSTRACT

This paper presents an overview of a flight test campaign performed at different test sites whose altitudes ranged from 0 to 7000 feet above mean sea level (AMSL) between September 2014 and February 2015. The purposes of this campaign were to: investigate the effects of altitude variation on noise generation, investigate the effects of gross weight variation on noise generation, establish the statistical variability in acoustic flight testing of helicopters, and characterize the effects of transient maneuvers on radiated noise for a medium-lift utility helicopter. In addition to describing the test campaign, results of the acoustic effects of altitude variation for the AS350 SD1 and EH-60L aircraft are presented. Large changes in acoustic amplitudes were observed in response to changes in ambient conditions when the helicopter was flown at constant indicated airspeed and gross weight at the three test sites. However, acoustic amplitudes were found to scale with ambient pressure when flight conditions were defined in terms of the non-dimensional parameters, such as the weight coefficient and effective hover tip Mach number.

LIST OF SYMBOLS

a_0	Ambient speed of sound at sea level
a_1	Ambient speed of sound at altitude
A_{cut}	Amplitude cutoff
C_W	Coefficient of weight
f_{cut}	Frequency cutoff
f_{MR}	Main rotor fundamental frequency
GW	Gross Weight
M_{AT}	Advancing tip Mach number
M_H	Hover tip Mach number
M_{H_e}	Effective hover tip Mach number
N_R	Non-dimensional rotor rotational speed
p'	Acoustic pressure
p'_n	Normalized acoustic pressure
P_0	Ambient static pressure at sea level
P_1	Ambient static pressure at altitude
$TOGW$	Takeoff Gross Weight
μ	Rotor advance ratio
ρ_0	Ambient air density at sea level
ρ_1	Ambient air density at altitude
Ω	Main rotor rotational speed
Ω_0	Nominal main rotor rotational speed

INTRODUCTION

Historically, the source noise data used in mission planning and community impact analyses have been measured at one altitude and then subsequently applied to make acoustic predictions at all altitudes. However, the ambient air density and temperature vary with the altitude above sea level, with well-known effects on the aerodynamic performance of the aircraft. Consequently, it should be expected that the aerodynamically-generated noise of helicopter rotors will also change in response to changes in the ambient conditions. These effects need to be quantified and considered when applying acoustic data acquired in one ambient condition to other ambient conditions.

Limited research has been conducted on the effects of changes in ambient conditions on helicopter noise generation. Boxwell et al. (Ref. 1), identified the governing non-dimensional parameters of rotor harmonic noise from theory and developed acoustic scaling laws to relate noise measurements from model-scale rotors in wind tunnels to in-flight measurements of full-scale vehicles. These scaling laws suggest that if the non-dimensional governing parameters defining the rotor operating condition are held constant, the resulting noise radiation will scale with the ambient pressure. This ambient pressure scaling can be defined using the following expression:

$$p'_n = \frac{\rho_0 a_0^2}{\rho_1 a_1^2} p' = \frac{P_0}{P_1} p' \quad (1)$$

Unfortunately, for a constant airspeed, flight path angle, and gross weight (parameters used by helicopter operators and in acoustic mission planning tools), the non-dimensional parameters governing rotor noise generation will vary as the ambient conditions change. Greenwood and Schmitz, (Ref. 2), estimated the effects of changing ambient conditions on helicopter harmonic noise radiation for the dimensionally-defined flight conditions used by operators and existing mission-planning tools. These effects were estimated using a semi-empirical model of the Bell 206 helicopter built using the non-dimensional Fundamental Rotorcraft Acoustic Modeling

Presented at the Acoustics Session of the 72nd Annual American Helicopter Society Forum, May 2016. DISTRIBUTION STATEMENT A. Approved for public release.

from Experiments (FRAME) (Ref. 3). Significant changes in the amplitude and directivity of noise radiation were predicted as the ambient density and temperature varied. For example, Figure 1 shows the predicted variation in Blade-Vortex Interaction (BVI) noise with changes in altitude for a standard atmosphere. Not only do the noise radiation characteristics vary, they do so non-linearly with variations in altitude. Different variations were predicted for other rotor noise sources, such as thickness and steady-loading. These results imply that changes in the acoustic state of the helicopter with changing ambient conditions must be accounted for in order to make accurate noise predictions, and that it is unlikely that simple empirical noise models can be developed that capture these effects. While the physics-based FRAME method may be capable of generalizing measured noise data collected under one set of ambient conditions to another, data did not exist to validate this application of the method.

In a previous test, the NASA/Army flight vehicle acoustics team at NASA Langley Research Center (LaRC) collected acoustic data for helicopters of the same model across a limited range of density-altitudes and temperatures. The data show substantial variation in the magnitude and directivity of radiated noise as ambient conditions changed. Because the variation in altitude was incidental to other test objectives, the vehicle operating conditions and configuration were not selected specifically to provide scientific data on the changes in noise radiation with changes in ambient conditions. However, these data underscored the importance of quantifying and understanding these effects in future tests.

TECHNICAL APPROACH

NASA and the U.S. Army Aeroflightdynamics Directorate (AFDD) conducted a joint flight test campaign to acquire validation data for the modeling of altitude variations and maneuvers in FRAME. Testing occurred at three altitudes: Salton Sea, CA (sea level), Amedee, CA (4000 feet AMSL) and Sweetwater, NV (7000 feet AMSL) with two aircraft being tested at each site. These sites were selected to give as wide an altitude variation as possible while retaining the ability to operate the aircraft at similar weight coefficients and tip Mach numbers. The locations of the test sites are shown in Figure 2.

AIRCRAFT DESCRIPTION

The first aircraft tested was a 4000 pound Eurocopter AS350 SD1 operated by Aris Helicopters. The aircraft was originally manufactured by Eurocopter as an AS350 BA, and later modified by Soloy Aviation to the AS350 SD1 configuration, powered by a single Honeywell LTS101-600A-3A engine and shown in Figure 3. The aircraft was fitted with an air data boom built by NASA Ames to record angle of attack, sideslip, airspeed, and temperature. Boom information was recorded on a data logger mounted on the instrumentation pallet shown in Figure 4. Also mounted on the instrumentation pallet was the NASA Langley Aircraft Navigation and Tracking System (ANTS, Figure 5) which recorded GPS tracking, aircraft attitudes and rates, and supplied the UTC time to the data logger for instrumentation synchronization.

The second aircraft, shown in Figure 6, was a 4-bladed Sikorsky EH-60L Advanced QuickFix helicopter operated by Aeroflightdynamics Directorate (AFDD) out of NASA Ames and modified to make it similar to a standard UH-60L. An air data boom for angle of attack, sideslip, airspeed, and temperature was mounted on the aircraft. Research sensors were installed throughout the control system to record aircraft parameters such as control positions, engine parameters, airframe attitudes and rates. An Ashtech GPS system obtained aircraft position data. All these data streams were merged and recorded on a PC-based Airframe Data System (ADS). Also mounted in the aircraft was a NASA ANTS system.

GROUND INSTRUMENTATION

The acoustic data were acquired using NASA's Mobile Acoustic Facility. This facility consists of two trailers: one is used to control the flight test and the other to maintain the 36 Wireless Acoustic Measurement Systems (WAMS) used to record the acoustic signals. Each WAMS consists of a ground board, microphone, GPS receiver, and antenna (Figure 7). Coordinated Universal Time (UTC) is obtained from the GPS and was used to synchronize all microphone, aircraft, and weather information. The WAMS setup used for this test consisted of a 1/2 inch Falcon (B&K 4189) microphone inverted with the diaphragm 1/4 inch over a 15 inch round ground board. The microphone is offset from the center of the ground board to minimize the edge effects and is based on SAE Aerospace Recommended Practice ARP4055 (Ref. 4). The acoustic signals were acquired at 25,000 Hz at 16 bit resolution. Up to 27 of these systems were deployed at one time.

The primary microphone layout used for all sites for this series of tests is a linear array of 21 microphones. Additional microphones were used as required and depended on the testing site for number and placement.

An extensive set of weather measurements were made throughout the test. A tethered weather balloon system (Figure 8) was located near the control trailer and sufficiently far away from the flight path to not interfere with the aircraft. The ballon altitude was stationary such that the weather sonde was at the primary aircraft altitude (usually 200 feet) above ground level (AGL). The weather sonde data (wind speed, wind direction, temperature, pressure, humidity and density) were radioed to the control trailer and displayed in real time. The temperature profile was measured by placing three to four temperature sensors on the balloon tether. These sensors recorded temperature, pressure and humidity as function of UTC time for post processing. A ZephIR 300 portable IEC 60825-1 Class 1 eye-safe LIDAR system was also deployed during testing (Figure 9) and measured wind speed and direction at 12 heights up to 900 feet AGL. This LIDAR system was placed under the aircraft flight path from 3000 to 1000 feet before the reference microphone depending on each test location layout.

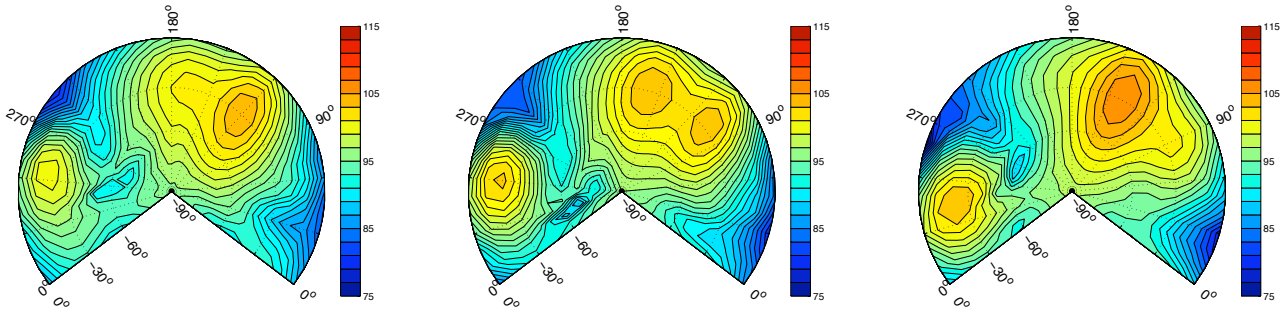

(a) Sea Level. (b) 5,000 feet AMSL. (c) 10,000 feet AMSL.

Fig. 1. The predicted variation in Blade-Vortex Interaction noise with change in International Standard Atmosphere (ISA) altitude for a Bell 206B in 60 Knots Indicated Airspeed (KIAS), -6 Flight Path Angle (FPA) descending flight (Ref. 2), scale is in BVISPL.

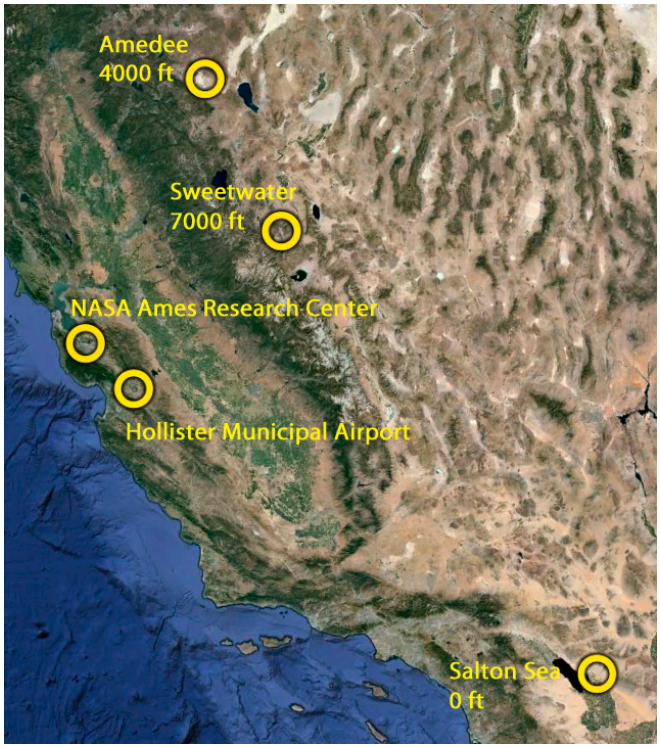

Fig. 2. Overview of testing sites.

Additionally, between 2 and 5 ground weather (GW) stations mounted at 4 feet AGL were placed among the microphone array. These ground weather stations recorded wind speed, wind direction, temperature, pressure, humidity and density.

Fig. 3. AS350 SD1 operated by Aris Helicopters during the campaign.

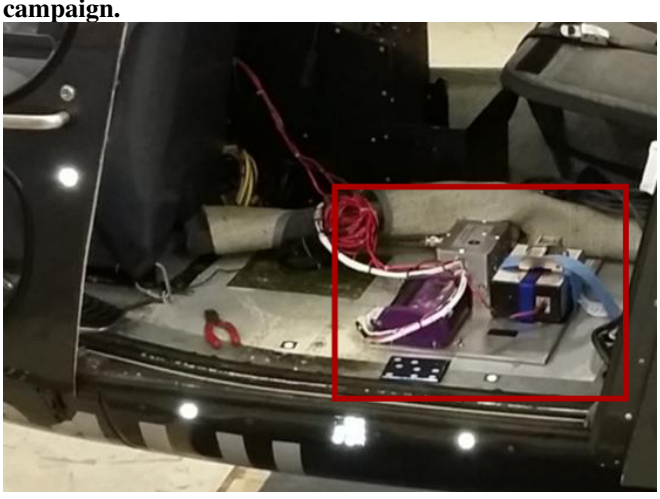

Fig. 4. Instrumentation pallet installed in AS350 SD1.

Fig. 5. NASA Langley Aircraft Navigation and Tracking System (ANTS).

Fig. 6. EH-60L operated by the US Army AFDD during the campaign.

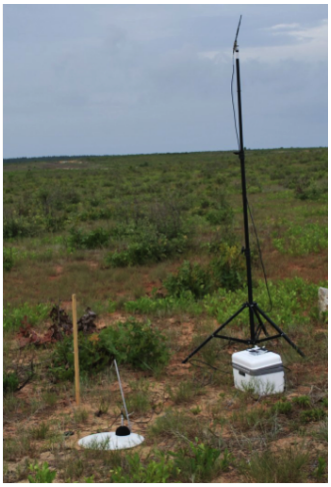

Fig. 7. Wireless Acoustic Measurement System.

Fig. 8. Tethered weather balloon with weather sonde.

Fig. 9. ZephIR 300 portable LIDAR system.

TESTING PHASES

The test campaign was performed in three test phases. The three test sites were chosen to have the widest possible density altitude variation and be near where the aircraft were based to minimize the ferry time of both aircraft to the test sites. NASA Ames Research Center was the base for the EH-60L. Riverside, CA and Hollister, CA were the two bases for the AS350 SD1. Historical weather data were examined for each of the three primary test sites, and the dates of testing at each site were selected to achieve similar ambient temperatures across all three sites. These locations are shown in Figure 2 and will be described in the following sections.

Hollister

The week before the first test phase was conducted, the boom installation, instrumentation checkout and calibration flight of the AS350 SD1 were performed at Hollister Municipal Airport, CA, where Aris Helicopters maintains a support facility. The boom was rap tested after installation and before the first flight to verify that the natural frequencies were within acceptable and safe levels.

Two airspeed calibration flights were performed after the aircraft instrumentation was installed. These consisted of flying upwind and downwind at airspeeds of 60, 80, 90, 100, and 110 knots. Descents were also performed at 80 knots at descent rates of 400, 900, and 1300 feet per minute. The data were used to develop calibration curves that were applied to the boom data.

Sweetwater, 7000 Feet

Phase I was performed at the Sweetwater USMC auxiliary airfield located near Bridgeport, CA. The land is owned by the National Park Service but used by the USMC under an agreement between the Marine Corp Mountain Warfare Training Center and the park service for C130 and troop training. Figure 10 shows the microphone positions, flight path over the microphones, weather balloon, control trailers, and LIDAR position at the Sweetwater test site. The microphone locations are listed in Table A1. Coordinate systems used in this report are with the origin at the microphone 11 position (referred to as the reference location), which is also the nominal aircraft crossing location. This table contains the X, Y and Z coordinates in feet from the GPS survey performed after microphone

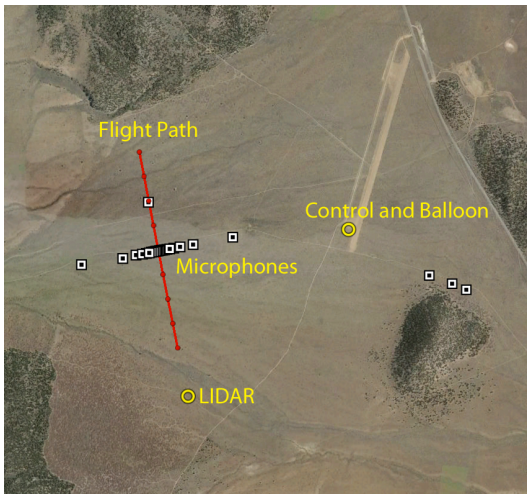

Fig. 10. Sweetwater test site, 7000 ft.

placement. This coordinate system has +X along the primary flight path, positive Y to the left of the flight path and Z is positive up. Additionally, Table A1 lists the non-microphone key locations.

Amedee, 4000 Feet

Phase II of the test was performed at Amedee Army Airfield located on the Sierra Army Depot, CA. Figure 11 shows the microphone positions, flight path over the microphones, weather balloon, control, and LIDAR position. The microphone locations are listed in Table A2. The coordinate system is defined as previously described as being centered at the reference location (microphone 11).

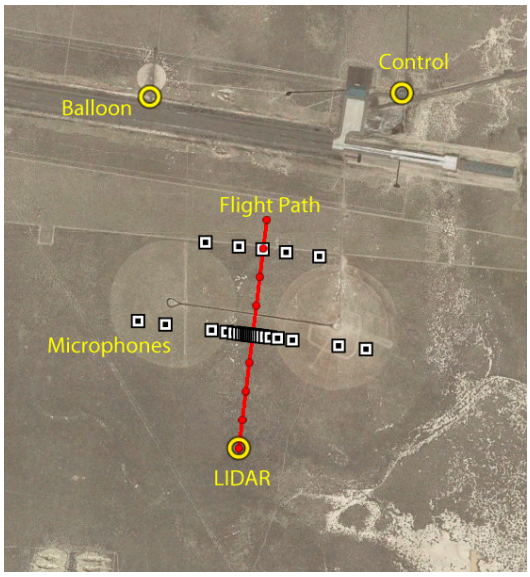

Fig. 11. Amedee test site, 4000 ft.

Salton Sea, 0 Feet

Phase III was performed at the U.S. Navy training facility Camp Billy Machen located at Salton Sea near Niland, CA. Yuma Proving Grounds provided test range coordination. Figure 12 shows the microphone positions, flight path over the microphones, weather balloon, control, and LIDAR position. The microphone locations are listed in Table A3. The coordinate system is defined as previously described as being centered at the reference location (microphone 11).

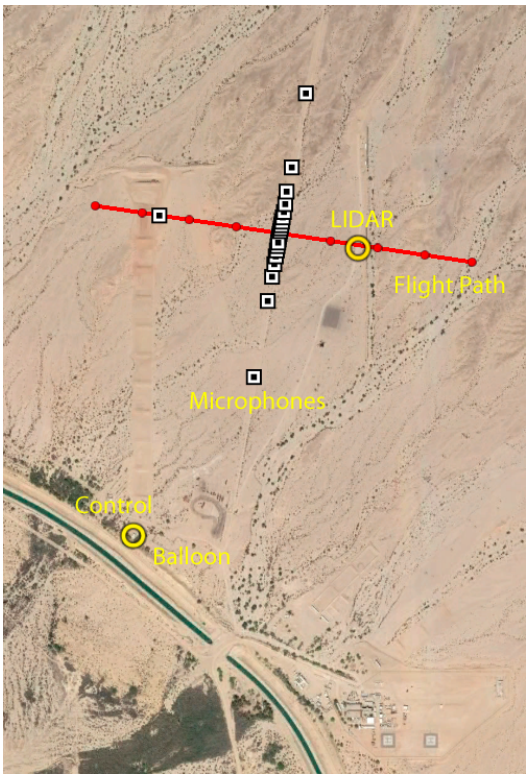

Fig. 12. Salton Sea test site, 0 ft.

TEST CONDITIONS

Altitude Variation Conditions

In order to measure the effects of changes in ambient conditions due to altitude variations (i.e. air density and temperature) on rotor noise generation, the flight conditions of the helicopters were defined in two different ways: dimensionally and non-dimensionally.

The first set of flight conditions were defined in terms of a constant indicated airspeed and flight path angle, the dimensional parameters typically used by pilots and mission planners, and used to define conditions in previous acoustic flight tests. For each aircraft, three of these conditions were defined—one moderate speed level flight condition, one high speed level flight condition, and one moderate speed descending flight condition. By holding these dimensionally-defined flight conditions constant at all three test sites, the effects of

changing altitude on noise radiation were directly measured for the manner in which helicopters are typically flown.

The second set of flight conditions were defined non-dimensionally using the parameters that are believed to govern the acoustic state of the helicopter's rotors. These governing parameters include the advance ratio, μ, and the advancing tip Mach number, M_{AT}. Based on real-time measurements of the ambient density and temperature at the flight altitude, the dimensional flight condition of the helicopter was carefully adjusted to match these parameters for each run. For the EH-60L, the indicated airspeed and rotor speed, $N_R = \Omega/\Omega_0$, were varied to match the specified values for advance ratio and advancing tip Mach number. However, precise rotor speed control was not available on the AS350 SD1; consequently, it was not possible to match both the advance ratio and advancing tip Mach number with variations in air temperature. Instead, the non-dimensional flight conditions for the AS350 SD1 were defined in terms of Gopalan's effective hover tip Mach number (M_{H_e}) as defined in Ref. 5. The effective hover tip Mach number is the hover tip Mach number (M_H) adjusted for Doppler amplification due to forward flight, and was identified by Gopalan as the key scaling parameter for rotor thickness noise. The effective hover tip Mach number can be expressed in terms of the rotor advance ratio, μ, and advancing tip Mach number, M_{AT}, using the expression:

$$M_{H_e} = \frac{M_{AT}}{1+\mu\,(1-M_{AT})} \tag{2}$$

The effective hover tip Mach number will match for all flight conditions where both the advancing tip Mach number, M_{AT}, and advance ratio, μ, are matched, such as those flown by the EH-60L. For the AS350 SD1, where N_R is held constant, the indicated airspeed required to match M_{H_e} will be between the airspeeds required to match μ and M_{AT}. Throughout the flight test campaign, each aircraft cycled through the six dimensionally and non-dimensionally defined flight conditions over the duration of flights, so that test points were sampled evenly across the daily variations in ambient conditions.

In addition to matching the dimensional or non-dimensional parameters that define a flight condition, the takeoff gross weight of the vehicle (TOGW) was varied at the start of each data collection flight. For each vehicle, flights were conducted at a baseline TOGW that did not vary with test site altitude. Additional flights were conducted using a TOGW selected for each site to match the main rotor weight coefficient (C_W) as air density varied. Thus, noise data were collected across a wide range of C_W for each vehicle due to fuel burn throughout the flight and TOGW variations.

The condition numbers are specified in Table A4 for the AS350 SD1 and Table A5 for the EH-60L. The target non-dimensional parameters are summarized in Table A6.

Steady Flight Source Noise Conditions

Steady state source noise characterization data were also acquired for both aircraft. The level flight conditions were performed at 150 feet AGL. Descents were initiated at an altitude such as to intersect the ground midway between the primary and secondary arrays. The aircraft initiated the descent such that the aircraft was in a constant descent rate and established on the flight path 3000 feet before the primary array. Minimal control inputs were performed after a steady condition was reached, but the pilot maintained the flight path and descent rate. The aircraft terminated the run in sufficient time to remain above 50 feet AGL. The conditions flown for source noise acquisition for the AS350 SD1 were level flight at 60, 70, 80, 90, 100, 120 KIAS; 3° , 6° , 9° descents at 60, 80, and 100 KIAS but were acquired over the full test with some at each site. The EH-60L source noise was all acquired at the Amedee test site. It consisted of level flight speed sweeps at 50 to 140 KIAS at both 96.5% and 100% N_R. Climb at 80 KIAS and descents from -3° to -12° were also performed at both N_R's. Table A7 summarizes these test conditions.

Steady level flight constant bank angle turns were flown over the linear ground array with the EH-60L. The methodology is shown conceptually in Figure 13. To perform this condition, the helicopter approached parallel to the array and offset from the array line the distance of the radius of the turn being flown. The turn was initiated such that it was stabilized by the time a heading 45 degrees offset from the flight line was obtained with the goal of crossing the reference microphone. The pilot maintained the designated angle of bank (15 or 30-degrees), maintaining a constant airspeed in the range of 50 to 100 KIAS at 200 foot AGL throughout the steady portion of the turn. The steady portion of the turn was maintained for at least 90 degrees of heading change. The aircraft then exited the turn parallel to the microphone array. Both left and right hand turns were flown. The steady turn condition codes and flight conditions are specified in Table A8.

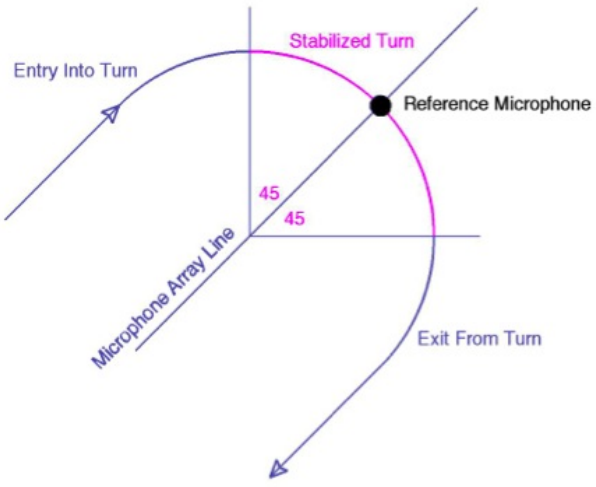

Fig. 13. Steady turn test technique diagram.

Maneuver Conditions

The rapidly changing aerodynamics of a maneuvering helicopter can significantly change the acoustic emissions of that aircraft. This was extensively investigated in 2011 on a Bell Model 430 helicopter and is reported in Ref. 6. However, the 2011 effort was performed on a light aircraft and focused on single control inputs. To further validate the FRAME maneuver prediction capabilities on more complex maneuvers and on a heavier, more modern aircraft, several days of data acquisition were dedicated to acquiring maneuver acoustics of the EH-60L. In general, the pilot approached the linear array at 100 feet AGL and executed the maneuver 2000 feet before the primary array. The maneuvers included constant speed banks, accelerating and decelerating banks, climbing turns, and quick stops. The intent was to not only gather data to understand the noise generation mechanisms for maneuvers, but to also investigate quieter ways to achieve the same flight path. An overview of the maneuver conditions is presented in Tables A9 thru A12.

ALTITUDE VARIATION RESULTS

A total of 1510 data runs were acquired at the three sites in 65.5 data acquisition flight hours (135 total flight hours including all ferry and instrumentation checkout flights). Table A13 provides a summary of the NASA and Army flight and run numbers, nominal takeoff weights and data type taken for both aircraft at all three testing sites. Because there was no ability to set the RPM for the AS350 SD1, the effective hover tip Mach number (M_{H_e}, Eq. 2) was targeted instead. Figure 14 plots the target M_{H_e} in magenta for the non-dimensionally defined conditions as it varies with μ and M_{AT} for constant rotor RPM under different ambient temperatures. Figures 14 and 15 show the advance ratio (μ) versus advancing tip Mach number (M_{AT}) for all V series test points. Therefore, while the target M_{H_e} was tightly held for the non-dimensionally defined conditions, the advance ratio spread is fairly large for that aircraft. However, the RPM was selectable for the EH-60L, and it can be seen that with real time control of RPM and airspeed that the target non-dimensional parameters (shown as the solid lines) can be achieved.

AS350 SD1 Level Flight V1 Thru V4

The harmonic averages (Ref. 7) of 60 main rotor pulses centered at an elevation of 15° down and 180° azimuth for the V1 thru V4 conditions at all three test sites for the AS350 SD1 are shown in Figures 16 and 17. These main rotor pulse pressures were normalized as per equation 1. All the harmonically averaged pulses are plotted in black with the average of the harmonically averaged pulses being plotted in yellow. The minimum value of the yellow line is displayed, and the number of runs contained on the graph is also shown. To minimize the weight variation effects, only the data runs that fell within the range of the nominal GW $\pm$ 5% for V1 and V3; and the nominal C_W $\pm$ 5% for V2 and V4 are included in the results shown

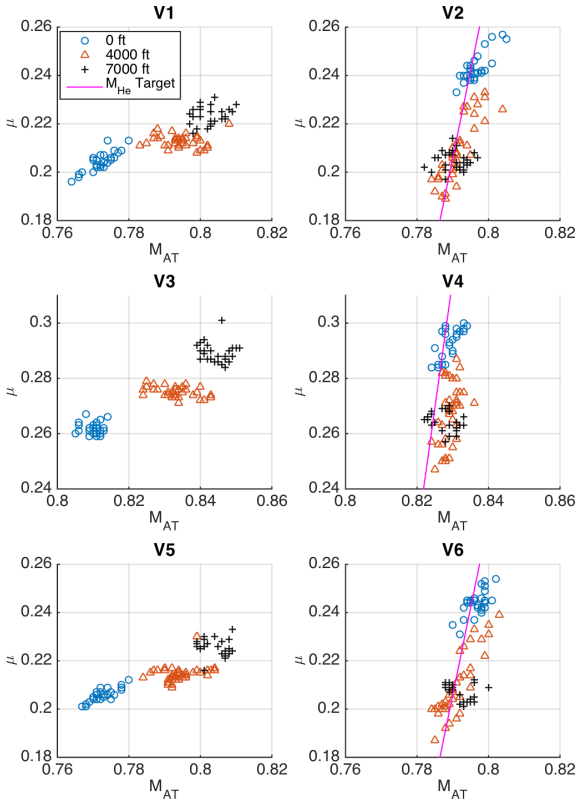

Fig. 14. μ vs M_{AT} for AS350SD1.

in the paper. For the dimensionally-flown conditions (V1 and V3), there is a significant increase in the amplitude with increasing altitude. For the moderate speed case, a 72% increase in amplitude (4.7 dB) is observed between the sea level and 7000 ft altitude test sites. The pulse amplitudes nearly double (5.4 dB) between these test sites for the high speed case. These results are consistent with the thickness noise trends identified in (Ref. 2), where a 5 dB increase in the inplane thickness noise over 7000 ft of altitude change was predicted for constant 100 knots indicated airspeed flight. In that paper, the primary cause of this increase in thickness noise was identified as the increase in tip Mach number as air density decreases, requiring a higher advance ratio be flown to maintain the same indicated airspeed. Conversely, much smaller changes are observed for the non-dimensionally flown conditions (V2 and V4) in accordance with Boxwell et al. (Ref. 1). Additionally, these figures show the high data repeatability between test runs achieved by harmonically averaging the data and tightly controlling the flight condition of the helicopter.

The normalized negative peak values for all flight conditions within the nominal GW $\pm$ 5% (for V1 and V3) and C_W $\pm$ 5% (for V2 and V4) range are plotted versus time in Figure 18. These values show the anticipated trend of increasing negative peak value with higher M_{H_e}. For an observer directly ahead of the rotor, the following monopole noise scaling relationship can be inferred from Gopalan's thickness noise

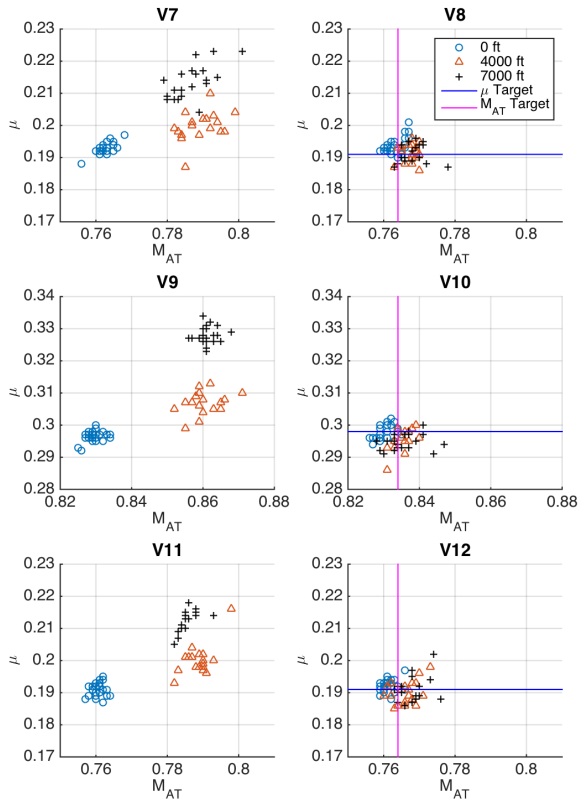

Fig. 15. μ vs M_{AT} for EH60L.

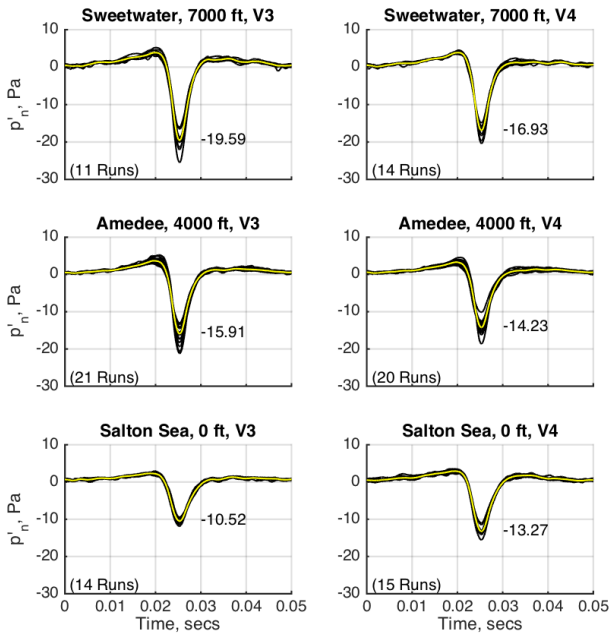

Fig. 17. Averaged AS350 SD1 main rotor pulse acoustic pressure for mid C_W data runs of conditions V3 and V4, 15° elevation angle.

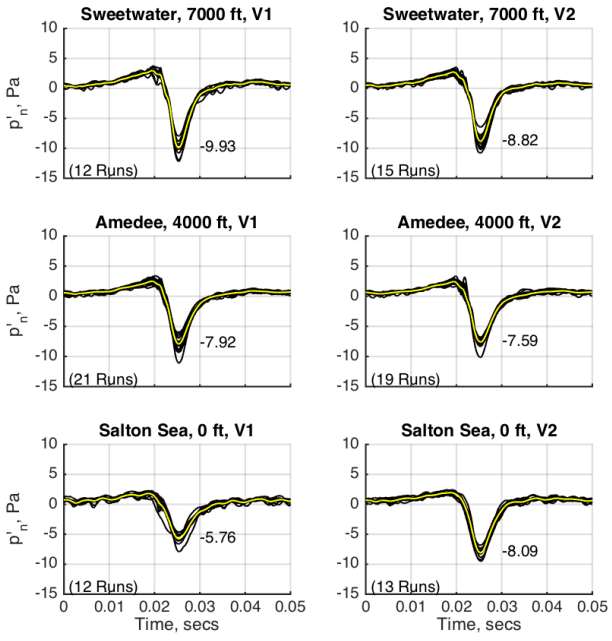

Fig. 16. Averaged AS350 SD1 main rotor pulse acoustic pressure for mid C_W data runs of conditions V1 and V2, 15° elevation angle.

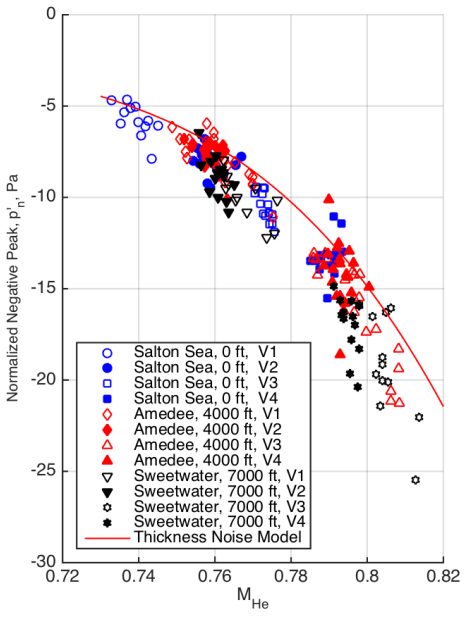

Fig. 18. AS350 SD1 negative peak values for mid C_W for conditions V1 thru V4.

approximation (Ref. 5):

$$p'_n \propto \frac{M_{H_e}^3}{r}\left[(3-M_{H_e})+5\mu\left(3-3M_{H_e}+M_{H_e}^2\right)\right] \qquad (3)$$

A least-squares fit was used to scale this expression to best fit the measured data, producing the solid line plotted in Figure 18. Comparison of the negative normalized peak values with the predicted curve indicates that the monopole thickness noise model is underpredicting the measured values at high advancing tip Mach numbers. Statistical analysis of the data was performed on these level flight negative peak values for each of the test sites and is shown in Figure 19. On each box in this

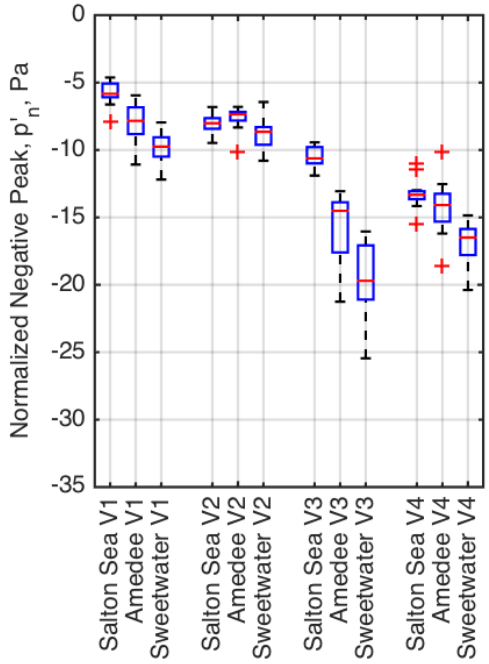

Fig. 19. AS350 SD1 negative peak median values for mid weights for conditions V1 thru V4.

figure, the central mark is the median, the top and bottom of the box are the 25th and 75th percentiles, the whiskers extend to the most extreme data points not considered outliers, and outliers are plotted individually as red pluses. The median, mean and standard deviations for each set of level flight data are shown in Table A14. Two significant trends are seen. The first observed trend is that the peak amplitude varies less with ambient conditions (altitude) for the non-dimensional flight conditions (V2, V4) than for the dimensional (IAS and GW) flight conditions (V1, V3). The second is that the deviation is less for the non-dimensional flight conditions than it is for the constant IAS conditions. A similar analysis was performed on the EH-60L level flight conditions (V7, V8, V9 and V10) and is shown in Figure 20 with the median, mean and standard deviation listed in Table A15 . The data presented for the EH-60L have been divided by a constant such that the amplitude values are obscured but the relative values are maintained. The data from the EH-60L show the same trends as the data from the

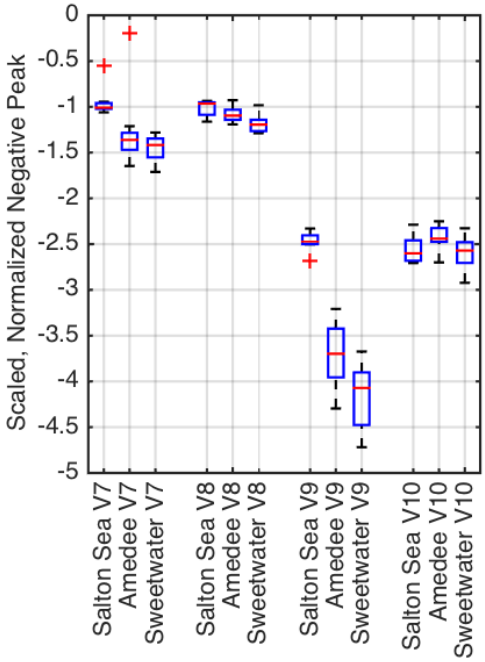

Fig. 20. EH60L scaled median values for mid weights for conditions V7 thru V10.

AS350 SD1. Thus, these observations lead to the conclusion that if data taken from one ambient condition are to be applied at a significantly different ambient, then the data should be applied using a non dimensional flight condition methodology.

Blade-Vortex Interaction Noise

The Blade-Vortex Interaction (BVI) noise was examined to identify changes with variations in ambient conditions. BVI noise is analyzed here using the wavelet-based extraction technique described in Stephenson and Greenwood (Ref. 8), whereby BVI noise is extracted by identifying acoustic signals above a pre-determined cutoff frequency (f_{cut}) and amplitude (A_{cut}) relative to the amplitude in the main rotor harmonic. For the AS350 SD1 vehicle, the cutoff parameters were chosen with a frequency cutoff of 11 main rotor harmonics ($f_{cut} = 11\ f_{MR}$) and amplitude cutoff of -6 dB ($A_{cut} = -6$ dB), consistent with the values chosen in Reference 8.

Figure 21 shows the Lambert projection of averaged peak-to-peak BVI pressure levels for the 80 knots indicated airspeed (V5) flight condition taken at each test location. We can see from this figure that the amplitude of BVI noise varied between runs at different ambient conditions.

Variations in BVI noise can be examined further by extracting the peak-to-peak pressures during specific vehicle flight conditions, vehicle parameters, and sound directivities. In this vein, a series of filters has been applied to the BVI data to ensure that BVI pulses from only the specified conditions are kept for further analysis. The data filter range was based off the dimensional (V5) and non-dimensional (V6) instantaneous values of the vehicle's weight, position, speed, and flight

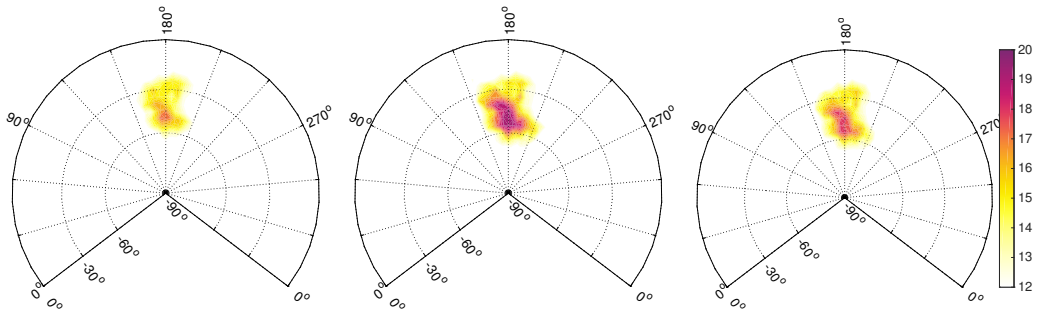

(a) Salton Sea, 0 ft (b) Amedee, 4000 ft (c) Sweetwater, 7000 ft

Fig. 21. BVI peak-to-peak variations with location for AS350 SD1, 80 KIAS descent condition (V5) in normalized pascals.

path angle. The filter values for the AS350 SD1 are provided in Table A16. Each individual peak-to-peak BVI pulse that matches the conditions in Table A16 has been corrected for static pressure and processed using the same statistical methods that produced Figure 19. The results of this process are shown in Figure 22. The statistical analysis identified more

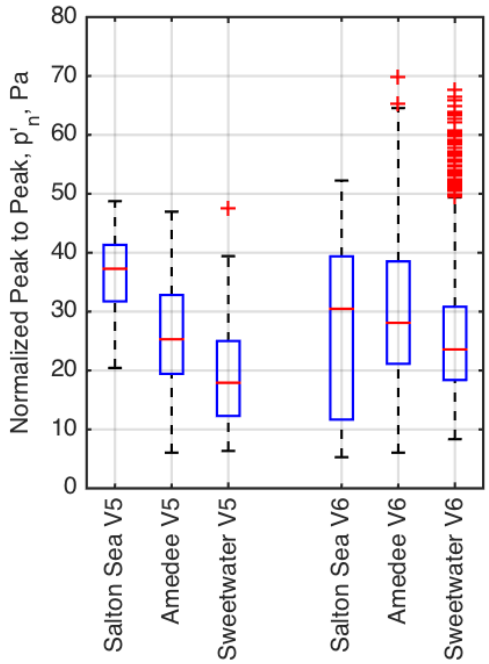

Fig. 22. AS350 SD1 peak-to-peak BVI values for mid C_W range, filtered by the parameters provided in Table A16.

outliers in Figure 22 than in Figure 19. This is due to each BVI pulse being accounted for individually, instead of the 60 rotor revolution averaged negative peak values used for the level flight conditions . Each filtered descent condition resulted in hundreds of individually assessed BVI occurrences.

The dimensional way of flying constant indicated airspeed and gross weight results in a trend for BVI amplitudes counter to what was seen before. In Figure 22, it is seen that increasing altitude for the dimensionally defined flight condition (V5) results in decreased BVI severity, where previously the negative thickness pulse amplitudes increased. However, consistent with previous results, the BVI pulses remain relatively constant when the full non-dimensional flight conditions are matched (V6). This result is consistent with the BVI noise trends identified in Ref. 2. In that paper it was shown that BVI noise levels could increase or decrease with changing ambient conditions, as changes in the rotor advance ratio, weight coefficient, and tip Mach numbers result in changes to the rotor wake geometry, with complex and non-linear effects on BVI noise radiation.

Figure 23 shows a similar pattern for BVI noise for the EH-60L descent data when processed with the filter values in Table A17. The EH-60L increasing altitudes produce decreasing

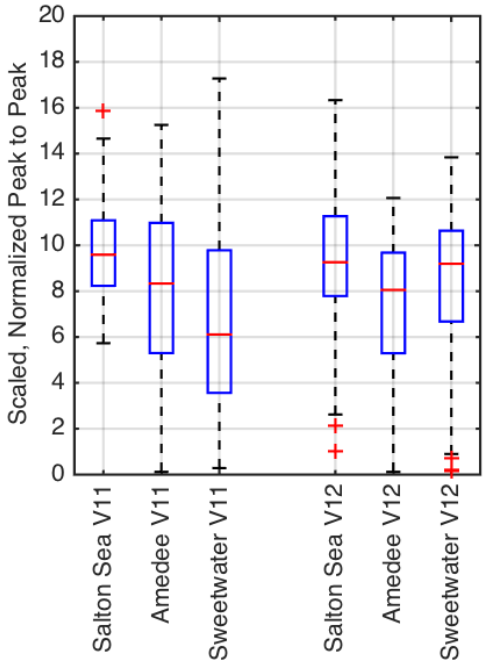

Fig. 23. EH-60L scaled peak-to-peak BVI values for mid weight range, filtered by the parameters provided in Table A17.

BVI severity for the dimensionally defined descent condition (V11), while the non-dimensionally defined condition (V12)

remains relatively constant although with a larger value range. Table A18 lists the median, mean, and standard deviation for the BVI analysis of the AS350 SD1 and the EH-60L.

CONCLUSIONS

A cooperative flight test campaign between NASA and the U.S. Army was performed between September 2014 and February 2015. The purposes of the testing were to: investigate the effects of altitude variation on noise generation, investigate the effects of gross weight variation on noise generation, establish the statistical variability in acoustic flight testing of helicopters, and characterize the effects of transient maneuvers on radiated noise for a medium-lift utility helicopter. This test was performed at three test sites (Salton Sea, 0 feet; Amedee, 4000 feet; and Sweetwater, 7000 feet). Two aircraft (AS30 SD1 and EH-60L) were tested at each site. A total of 165 flight hours were flown with 65 of those being data acquisition hours used to acquire 1510 data points.

The measured data confirm that changes in ambient conditions due to changes in altitude above sea level can result in significant changes in the radiated noise of helicopters when the flight conditions are defined in the dimensional terms typically employed by operators and mission planners. Consistent with theory, thickness noise radiated in-plane increases with decreasing air density and temperature. Changes in amplitude as great as 5.4 dB over 7000 ft altitude variation were observed. Significant changes in BVI noise were also observed in response to altitude variation; in general, BVI noise levels were seen to decrease with increasing altitude, although this trend is probably dependent on the specific indicated airspeed and flight path angle selected to define the flight condition.

The data also confirm that when flight conditions are defined in terms of the non-dimensional parameters thought to govern rotor harmonic noise radiation, the noise radiated under different ambient conditions may be scaled to a common static pressure with good agreement. This has strong implications for future acoustic flight testing, noise modeling, and mission planning. Helicopter operating conditions should be classified using non-dimensional parameters, allowing data collected under one set of ambient conditions to be generalized to other ambient conditions. Care must be taken during data collection to capture enough variation in these parameters in order to model helicopter noise radiation over the practical operating range of the helicopter. Helicopter acoustic mission planning tools can then lookup such data on a non-dimensional basis, applying to the ambient conditions specific to the time and location of planned operations. Existing mission planning tools, formulated on a dimensional basis, may introduce significant errors in acoustic levels when applying measured or predicted noise data for one set of ambient conditions to another.

REFERENCES

[1]Boxwell, D. A., Schmitz, F. H., Splettstoesser, W. R., and Schultz, K. J., "Model Helicopter Rotor High-Speed Impulsive Noise: Measured Acoustics and Blade Pressures," NASA TM 85850, September 1983.

[2]Greenwood, E. and Schmitz, F. H., "Effects of Ambient Conditions on Helicopter Rotor Source Noise Modeling," *Journal of Aircraft*, Vol. 51, (1), January 2014, pp. 90–103. doi: 10.2514/1.C032045

[3]Greenwood, E., *Fundamental Rotorcraft Acoustic Modeling From Experiments (FRAME)*, Ph.D. thesis, University of Maryland, College Park, MD, January 2011.

[4]"SAE ARP4055, Ground-Plane Microphone Configuration for Propeller-Driven Light-Aircraft Noise Measurement," November 2007.

[5]Gopalan, G. and Schmitz, F. H., "Far-Field Near-In-Plane Harmonic Main Rotor Helicopter Impulsive Noise Reduction Possibilities," American Helicopter Society 64th Annual Forum, 2008.

[6]Watts, M. E., Greenwood, E., Smith, C. D., Snider, R., and Conner, D. A., "Maneuver Acoustic Flight Test of the Bell 430 Helicopter Data Report," NASA TM-2014-218266, May 2014.

[7]Greenwood, E. and Schmitz, F. H., "Separation of Main and Tail Rotor Noise from Ground-Based Acoustic Measurements," *Journal of Aircraft*, Vol. 51, (2), February 2014, pp. 464–472. doi: 10.2514/1.C032046

[8]Stephenson, J. H. and Greenwood, E., "Effects of Vehicle Weight and True Versus Indicated Airspeed on BVI Noise During Steady Descending Flight," American Helicopter Society 71st Annual Forum, May 2015.

ACKNOWLEDGEMENT

The authors would like to thank the team for their outstanding dedication and hard work that made this aggressive test possible. NASA Langley: Susan Gorton, Nikolas Zawodny, C. Benny Lunsford, Angela Williams. NASA Ames: Bill Warmbrodt, Gloria Yamauchi, Gina Willink, Benny Cheung, Robert Kufeld, Jim Kennon, Seth Kurasaki. U.S. Army: Ben Sim, David Conner, Ernesto Moralez, Zoltan Szoboszlay, Brian Fujizawa, Nathan Mielcarek, MAJ Joseph Minor, MAJ Joe Davis, LTC Carl Ott, Randy Watson, Rich Huber, Casey Blaskowski. Analytical Mechanics Associates: Charles Smith, H. Keith Scudder, Andrew Mccrea, Michael Walke. Aris Helicopters: Scott Donley, Samuel Nowden, Timothy West, Hector Ayala. USMC Mountain Warfare Training Center: HMC Gregory Highfill, CAPT Jonathan Geisler, CAPT Benjamin Hand. Sierra Army Depot: Lester Cooper, Jon France, Andrew McLarty, Dan Donovan. Yuma Proving Grounds: Brianna Carlson, J. Corey Milligan. Airfilm Camera Systems: Scott Herring

APPENDIX A: TABLES

Table A1. Sweetwater Locations

Mic Number	X, ft	Y, ft	Z, ft
1	-0.2	1532.1	93.5
2	-22.3	713.8	41.7
3	-2.5	444.4	25.9
4	-6.3	316.1	18.5
5	-6.8	236.8	14.3
6	-6.7	178.6	10.6
7	1.5	135.0	7.9
8	-0.4	93.8	5.8
9	2.6	56.6	3.2
10	2.1	26.9	1.6
11 (ref)	0.0	-0.0	0.0
12	4.2	-28.9	-1.6
13	3.3	-60.0	-3.2
14	1.6	-92.1	-5.3
15	0.3	-129.6	-6.9
16	2.1	-179.1	-9.5
17	-0.3	-235.6	-12.7
18	0.8	-318.0	-17.4
19	4.0	-445.5	-25.3
20	3.5	-710.5	-40.7
21	7.8	-1521.7	-86.6
24	994.5	11.0	-5.8
27	-1480.2	-5345.6	-280.9
28	-1908.7	-6048.7	-316.8
29	-1732.6	-5780.6	-303.1
LIDAR	-3012.4	-19.8	-84.8
Balloon	-169.9	-3937.6	-118.9
GW 2	47.3	-3.7	0.0
GW 4	32.6	-1564.6	-86.6
Control	-149.7	-3815.6	-115.9

Table A2. Amedee Locations

Mic Number	X, ft	Y, ft	Z, ft
1	-1.7	1519.1	-0.9
2	-2.8	705.8	0.1
3	0.7	442.4	-0.3
4	0.3	313.7	-0.2
5	-1.0	230.8	-0.1
6	1.1	171.8	-0.1
7	-1.5	125.9	0.1
8	2.5	88.8	-0.2
9	-1.2	55.0	0.1
10	-7.1	22.3	-0.1
11 (ref)	0.0	0.0	0.0
12	-1.1	-35.9	-0.1
13	-1.7	-66.7	-0.2
14	-0.9	-96.8	-0.2
15	0.3	-136.8	-0.2
16	-0.7	-179.2	0.0
17	-0.8	-239.3	0.0
18	-0.2	-325.6	0.1
19	-0.7	-454.8	0.2
20	-0.7	-715.3	0.4
21	-0.3	-1528.0	0.5
22	1488.6	988.1	-0.5
23	1497.7	415.1	-0.5
24	1487.3	-9.4	-0.3
25	1508.1	-416.7	0.3
26	1506.4	-1004.9	0.4
27	-1.5	2000.4	-0.9
28	0.2	-2009.8	0.2
LIDAR	-1993.8	1.3	5.3
Balloon	3872.6	2282.3	-0.2
GW 1	4441.2	-2108.9	-0.2
GW 2	0.2	-2009.8	0.2
GW 3	0.0	0.0	0.0
GW 4	-1.5	2000.4	-0.9
GW 5	1487.3	-9.4	-0.3
Control	4441.2	-2108.9	-0.2

Table A3. Salton Sea Locations

Mic Number	X, ft	Y, ft	Z, ft
1	37.9	1519.5	-15.2
2	15.5	711.1	-8.7
3	9.6	454.1	-5.2
4	6.4	320.2	-1.5
5	3.8	237.8	-0.5
6	2.2	174.4	0.1
7	1.3	129.1	0.1
8	0.7	91.5	0.6
9	0.5	59.2	-0.8
10	1.4	29.0	-0.5
11 (ref)	0.0	-0.0	0.0
12	-1.4	-29.0	0.1
13	-2.6	-59.2	0.5
14	-3.6	-92.0	1.0
15	-4.9	-129.6	1.6
16	-6.5	-175.1	2.5
17	-9.9	-232.6	2.6
18	-11.3	-315.5	3.8
19	-5.5	-446.3	15.6
20	-20.4	-703.3	18.0
21	-48.0	-1487.8	26.9
24	1277.8	3.4	-5.1
LIDAR	-801.7	18.3	7.7
Balloon	1370.0	2952.6	22.2
GW 1	1370.0	2952.6	22.2
GW 2	-168.9	-1503.5	26.9
GW 3	-127.1	34.9	-0.8
GW 4	-97.3	1571.5	19.6
GW 5	1290.4	1.1	-5.9
Control	1370.0	2952.6	22.2

Table A4. AS350 SD1 Altitude Variation V Condition Codes

Condition Code	KIAS	FPA °	Description
V1	80	0	Commanded
V2	80(1)	0	Match M_{H_e} and C_W
V3	105	0	Commanded
V4	105(1)	0	Match M_{H_e} and C_W
V5	80	-6	Commanded
V6	80(1)	-6	Match M_{H_e} and C_W

(1) Airspeed determined at time of point acquisition

Table A5. EH-60L Altitude Variation V Condition Codes

Condition Code	KIAS	FPA °	Description
V7	80	0	Commanded
V8	80(1)	0	Match μ, M_{AT} and C_W
V9	125	0	Commanded
V10	125(1)	0	Match μ, M_{AT} and C_W
V11	80	-6	Commanded
V12	80(1)	-6	Match μ, M_{AT} and C_W

(1) Airspeed, RPM determined at time of point acquisition

Table A6. Altitude Variation V Target Conditions

Parameter	AS350 Low	AS350 High	EH-60L Low	EH-60L High
μ	-	-	0.191	0.298
M_H	-	-	0.642	0.642
M_{AT}	-	-	0.764	0.834
M_{H_e}	0.762	0.794	0.731	0.794
C_W	0.00384	0.00384	0.0075	0.0075

Table A7. AS350 SD1 and EH-60L Straight Steady State Conditions

KIAS	6	3	0	-3	-6	-9	-12
40			A				
50			E	E	E	E	E
60			A	A	A	A	
65			E	E	E	E	E
70			A				
80	E	E	E	A, E	E	A, E	E
90			A				
95			E	E	E		
100			A	A			
110			E	E			
120			A, E				
130			E				
140			E				

A: AS350 SD1

E: EH-60L 100% and 96.5% N_R

Table A8. EH-60L Steady Turns

		Bank Angle	
KIAS	Direction	15°	30°
65	Left	S3	S4
	Right	S1	S2
95	Left	S7	S8
	Right	S5	S6

Table A9. EH-60L Constant Speed Banks

		Bank Angle	
KIAS	Direction	20°	30°
65	Left	M9	M12
	Right	M3	M6
80	Left		M44
	Right		M43
95	Left	M8	M11
	Right	M2	M5
110	Left	M7	M10
	Right	M1	M4

Table A10. EH-60L Accelerating and Decelerating Banks

Aggression	Direction	80 KIAS Start Accel	120 KIAS Start Decel
Moderate	Left	M20	M24
	Right	M18	M22
Aggressive	Left	M21	M25
	Right	M19	M23

Note: Initiate accel/decel at -3000 then bank at -2000 ft

Table A11. EH-60L Climbing Turns

		Climb Angle	
KIAS	Direction	3°	6°
80	Left	M27	M33
	Right	M26	M32
95	Left	M29	M35
	Right	M28	M34
110	Left	M31	M37
	Right	M30	M36

Note: Initiate climb at -3000 then bank at -2000 ft

Table A12. EH-60L Quick Stop

KIAS	Aggression	
95	Moderate	M13
	Aggressive	M14

Table A13. Altitude Variation Test Run Summary

Site	AC	Date	Nom TOGW	Data Type
Sweet-water (7000')	AS350	9/30/14	4400	V
		10/1/14	3915	V
		10/2/14	3915	V, L
	EH-60L	10/6/14	18500	V
		10/7/14	16500	V
		10/8/14	16500	V
Amedee (4000')	AS350	10/28/14	4090	V,L
		10/29/14	4400	V
		10/30/14	4650	V
	EH-60L	11/6/14	18500	V
		11/6/14	18500	V, M
		11/7/14	18500	M
		11/7/14	18500	M
		11/8/14	18500	L
		11/8/14	18500	V
		11/10/14	18500	L, A
		11/10/14	18500	L, A
		11/11/14	18500	A
		11/11/14	18500	A
		11/12/14	18500	M
		11/12/14	18500	M
		11/14/15	18500	M, S
		11/14/14	18500	M
Salton Sea (0')	EH-60L	2/7/15	21350	V
		2/7/15	21350	V
		2/7/15	21350	V
		2/8/15	18500	V
		2/8/15	18500	V
		2/8/15	18500	V
		2/9/15	16500	V
		2/9/15	16500	V
	AS350	2/13/15	4630	V
		2/14/15	4630	V, A
		2/14/15	4400	V, L
		2/15/15	4400	V
		2/16/15	4400	V

V: Altitude Variation Condition
M: Maneuver Condition
L: Level Flight Condition
A: Approach Condition
S: Steady Turn Condition

Table A14. AS350 SD1 Level Flight Negative Peak Statistics

Location	Condition	Median	Mean	Std. Dev.
Salton Sea	V1	-5.83	-5.76	0.91
	V2	-8.01	-8.09	0.75
	V3	-10.62	-10.52	0.82
	V4	-13.32	-13.27	1.04
Amedee	V1	-7.84	-7.92	1.26
	V2	-7.35	-7.59	0.75
	V3	-14.51	-15.91	2.77
	V4	-14.08	-14.23	1.72
Sweetwater	V1	-9.75	-9.93	1.26
	V2	-8.65	-8.82	1.08
	V3	-19.70	-19.59	2.79
	V4	-16.49	-16.93	1.58

Table A15. EH-60L Level Flight Scaled Negative Peak Statistics

Location	Condition	Median	Mean	Std. Dev.
Salton Sea	V7	-1.01	-0.94	0.18
	V8	-0.96	-1.01	0.09
	V9	-2.47	-2.47	0.11
	V10	-2.60	-2.55	0.15
Amedee	V7	-1.36	-1.31	0.33
	V8	-1.10	-1.09	0.07
	V9	-3.70	-3.71	0.35
	V10	-2.44	-2.43	0.13
Sweetwater	V7	-1.42	-1.45	0.13
	V8	-1.19	-1.18	0.11
	V9	-4.07	-4.16	0.33
	V10	-2.57	-2.60	0.18

Table A16. AS350 SD1 parameter filters for BVI statistical analysis.

Parameter	V5 Condition	V6 Condition
Azimuth	$180° \pm 5°$	
Elevation	$-45° \pm 5°$	
Flight Path Angle	$-6° \pm 1°$	
GW [lbs]	$4050 \pm 5\%$	N/A
C_W	N/A	$0.00384 \pm 5\%$
KIAS	80 ± 5	N/A
M_{H_e}	N/A	$0.762 \pm 5\%$

Table A17. EH-60L parameter filters for BVI statistical analysis.

Parameter	V11 Condition	V12 Condition
Azimuth	$180° \pm 5°$	
Elevation	$-45° \pm 5°$	
Flight Path Angle	$-6° \pm 1°$	
GW [lbs]	$17,250 \pm 5\%$	N/A
C_W	N/A	$0.00735 \pm 5\%$
KIAS	80 ± 5	N/A
M_{AT}	N/A	$0.764 \pm 5\%$

Table A18. BVI Peak-to-Peak Statistics

Location	Condition	Median	Mean	Std. Dev.
Salton Sea	V5	37.27	36.53	6.34
	V6	30.47	26.99	14.03
	V11	9.59	9.71	1.90
	V12	9.26	9.41	2.73
Amedee	V5	25.31	25.68	9.21
	V6	28.09	30.84	13.94
	V11	8.33	8.01	3.71
	V12	8.05	7.39	2.98
Sweetwater	V5	17.92	19.20	7.81
	V6	23.59	26.55	12.40
	V11	6.11	6.68	4.00
	V12	9.20	8.29	3.16